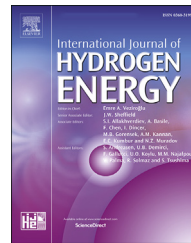




ELSEVIER

Available online at [www.sciencedirect.com](http://www.sciencedirect.com)  
**ScienceDirect**

journal homepage: [www.elsevier.com/locate/he](http://www.elsevier.com/locate/he)

# Hydroxyapatite supported Pd<sub>x</sub>In<sub>100-x</sub> as a novel electrocatalyst for high-efficiency glucose electrooxidation

Berdan Ulas <sup>a,\*</sup>, Yonca Yilmaz <sup>b</sup>, Serap Koc <sup>c</sup>, Hilal Kivrak <sup>d,e</sup>

<sup>a</sup> Department of Mining Engineering, Faculty of Engineering, Van Yuzuncu Yil University, Van, 65000, Turkey

<sup>b</sup> Department of Chemical Engineering, Faculty of Engineering, Van Yuzuncu Yil University, Van, 65000, Turkey

<sup>c</sup> Department of Mechanical Engineering, Faculty of Engineering, Van Yuzuncu Yil University, Van, 65000, Turkey

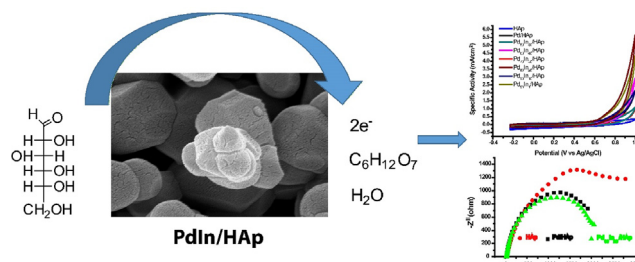
<sup>d</sup> Department of Chemical Engineering, Faculty of Engineering and Architectural Science, Eskisehir Osmangazi University, Eskisehir, 26040, Turkey

<sup>e</sup> Translational Medicine Research and Clinical Center, Eskisehir Osmangazi University, 26040, Eskisehir, Turkey

## HIGHLIGHTS

- PdIn/HAp catalysts with varying atomic molar ratios were synthesized by the NaBH<sub>4</sub> reduction method.
- Pd<sub>80</sub>In<sub>20</sub>/HAp exhibited excellent electrocatalytic activity for glucose electrooxidation.
- Pd<sub>80</sub>In<sub>20</sub>/HAp showed long-term stability as a DGFC anode catalyst.

## GRAPHICAL ABSTRACT



## ARTICLE INFO

### Article history:

Received 1 December 2021

Received in revised form

27 June 2022

Accepted 30 June 2022

Available online xxx

### Keywords:

Glucose

Electrooxidation

Palladium

Indium

Hydroxyapatite

Fuel cell

## ABSTRACT

Fuel cells are a very good candidate to provide energy conversion with green technology. Glucose is used as a fuel in fuel cells since it is easily available and has a high energy density. Herein, hydroxyapatite (HAp) was synthesized by precipitation method, and the sodium borohydride (NaBH<sub>4</sub>) reduction method was used to fabricate HAp supported PdIn (PdIn/HAp) alloy anode catalysts at varying atomic molar ratios for glucose electrooxidation. Structural, crystallographic, and morphological properties of the PdIn/Haps were determined with X-ray diffraction analysis (XRD), X-ray photoelectron spectroscopy (XPS), scanning electron microscope (SEM), Brunauer-Emmett-Teller (BET) analysis, transmission electron microscopy (TEM), and inductively coupled plasma mass spectrometry (ICP-MS). Electrochemical impedance spectroscopy (EIS), cyclic voltammetry (CV), and chronoamperometry (CA) were employed for the electrocatalytic activity and stability of PdIn/Haps toward glucose electrooxidation. The results show that HAp has a boosting effect for PdIn alloy towards glucose electrooxidation. Pd<sub>80</sub>In<sub>20</sub>/HAp showed 2.6 times

\* Corresponding author.

E-mail addresses: [berdanulas@yyu.edu.tr](mailto:berdanulas@yyu.edu.tr), [berdanulas2@gmail.com](mailto:berdanulas2@gmail.com) (B. Ulas).

<https://doi.org/10.1016/j.ijhydene.2022.06.314>

0360-3199/© 2022 Hydrogen Energy Publications LLC. Published by Elsevier Ltd. All rights reserved.

higher electrocatalytic activity than Pd/HAp, and it is the most active and stable catalyst in this study with a specific activity of 5.64 mA/cm<sup>2</sup>.

© 2022 Hydrogen Energy Publications LLC. Published by Elsevier Ltd. All rights reserved.

## Abbreviations

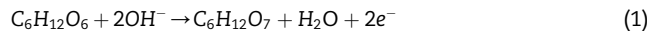
HAp	Hydroxyapatite
EIS	Electrochemical Impedance Spectroscopy
DGFC	Direct Glucose Fuel Cell
XRD	X-Ray Powder Diffraction
CV	Cyclic Voltammetry
BET	Brunauer–Emmett–Teller
CNF	Carbon Nanofiber
RGO	Reduced Graphene Oxide
SEM	Scanning Electron Microscope
EDX	Energy Dispersive X-Ray Analysis
ICP-MS	Inductively Coupled Plasma – Mass Spectrometer
CA	Chronoamperometry
GCE	Glassy Carbon Electrode
PEMFC	Polymer Electrolyte Membrane Fuel Cell
TEM	Transmission Electron Microscopes
MWCNT	Multi-Walled Carbon Nanotubes
CNF	Carbon Nanofiber
KB	Ketjenblack Carbon
r.d.s	Rate Determining Step
R	Resistance
W	Warburg Element
Q	Constant Phase Element
S <sub>BET</sub>	BET Surface Area
C	Concentration
D	Diffusion Coefficient
A	Surface Area

## Introduction

Fuel cells are devices that convert chemical energy into electrical energy through electrochemical reactions [1]. Their use in portable electronic devices, transportation, and constant power generation has become quite common. Automobile companies have produced prototype automobile models that provide energy from fuel cells [2,3]. Cost reduction is an important problem for fuel cells to become a widely used commercial product. However, proton exchange membrane fuel cells (PEMFC) and direct methanol fuel cells have promising performance for commercialization [4–6]. Apart from these, more studies should be conducted on liquid-feed fuel cells namely hydrazine [7,8], methanol [9,10], ethanol [11,12], glycerol [13,14], formate [15,16], formic acid [17,18], dimethyl ether [19], and glucose [20,21].

The negative effects of fossil fuel sources on environment and the human health have accelerated the research of

readily available and environmentally friendly materials for fuel cells [22–24]. Glucose is a good alternative for use as a fuel in fuel cells due to its unique properties among liquid fuels such as dimethyl ether, hydrazine, methanol, formic acid, and ethanol. Because glucose is a neutral carbon source, it can be stored and transported more safely than other fuels [25,26]. The fact that glucose is not toxic [27], flammable [28], and volatile [29] also reduces the storage and transportation costs of glucose. It is also a very good energy provider, releasing 24 e<sup>-</sup> in the complete oxidation of glucose [30,31]. The anode, cathode, and overall reactions for direct glucose fuel cells (DGFCs) are given in Eqns. (1)–(3) [32].



The kinetics of glucose electrooxidation reaction occurring at the anode is vital for improving the efficiency of DGFCs. The reaction kinetics slowing down, especially at low temperatures reduces the performance of the fuel cell. The performances of noble metals namely Pt and Pd as anode catalysts for DGFCs have been investigated before. However, many studies have reported that monometallic Pd and Pt are poisoned by carbonaceous intermediates formed during glucose electrooxidation [33–35]. Researchers have benefited from the synergistic effects of binary anode catalysts to increase poisoning tolerance. Accordingly, the electrocatalytic performance of anode catalysts for glucose electrooxidation have been reported such as NiCuO/ITO [36], NiO<sub>x</sub>/Gr/GCE [37], Ir/CNT [38], Pt/CNT [39], NiO<sub>x</sub>/GC [40], ITO/TiO<sub>2</sub>/Co<sub>3</sub>O<sub>4</sub> [41], Co@NCD [42], Mg<sub>65</sub>Bi<sub>35</sub> [43], BiAu/MWCNT [44], NiCu/GC [45], Pt<sub>9</sub>Bi<sub>1</sub>/C [46], Pd/C<sub>3</sub>N<sub>4</sub>–C [47], NiCo/rGO [1], AuPtPd [48], Bi–Co–S [49], Pd<sub>3</sub>Cu–B/C [29], NiFe/Graphene [50], PtNiCu/GC [51], Fe–Ni–Co/C [28], PdPt/Graphene [27], and PdIn/C [52]. There is extensive sensor literature as well as fuel cell applications on glucose electrooxidation. In recent years, Tsiakaras group investigated PdCo/KB [53] and Pd/N-3D [54] electrocatalysts for the detection of glucose co-existing with ascorbic acid, uric acid, and dopamine in the human body. This research group proposed mechanisms for glucose electrooxidation on Pt, Pd, Au, Cu, Co, and Ni, and the mechanism of glucose electrooxidation on Pd is shown in Scheme 1 [55,56]. Researchers reported that glucose electrooxidation activity is strongly dependent on charge and mass transport between metal (II) and metal (III).

These multi-metal catalysts have been reported to have higher electrocatalytic activity and stability than monometallic catalysts. Researchers have attributed the increased

electrochemical performance to bifunctional, electronic, and ensemble effects or a combination of these effects. In addition, many studies have emphasized the effect of atomic molar ratios of metals on their electrocatalytic activities. Chai et al. informed that the mass activity of the  $\text{Pd}_3\text{Cu}-\text{B/C}$  electrocatalyst for glucose electrooxidation was  $0.105 \text{ A/mg Pd}$ , which was approximately 15 times higher than compared to  $\text{Pd/C}$ . Researchers reported that the d band center of palladium shifted towards its optimum value with the addition of Cu [29]. Another factor affecting the performance of catalysts is the selection of support materials with which the particles can be well dispersed. As far as we know, carbon derivatives such as CNT, rGO, and XC-72 are frequently used as support materials for glucose electrooxidation. Researchers have reported that these carbon derivatives are preferred as support materials owing to their electrically conductive and high surface areas [57,58]. Since the carbon derivatives do not interact strongly enough with the metal nanoparticles loaded on them, the catalytic activity is negatively affected [59]. Hydroxyapatite (HAp) is a good alternative to the aforementioned carbonaceous support materials due to its abundance in nature and its hydroxyl-rich structure to which metal nanoparticles can bind [60]. The most important properties of Haps that allow them to be used as support materials are their high adsorption capacity and ion exchange capacity [61] as well as the easily adjustable Ca/P ratio [62]. Haps have an important potential as catalyst support material due to their easy design, flexible structures, thermal stability, adjustable surface acidic/basic properties, and bifunctionality because of acidic/basic sites [63,64]. Cui et al. reported that the  $\text{Pd/HAp}$  catalyst showed approximately two times higher electrocatalytic activity compared to  $\text{Pd/C}$  for ethanol electrooxidation and the enhancement in catalytic activity was attributed to the removal of adsorbed carbonaceous compounds by hydroxyl groups on the HAp surface [59]. Safavi et al. also informed that hydroxyl groups adsorbed on HAp surface in an alkaline medium increased electrocatalytic activity by preventing CO-like poisoning [65]. Haps have been frequently used as a component of composite materials for glucose sensors and medical applications. However, the performance of HAp, which has a high tolerance to CO poisoning with its hydroxyl-rich chemical structure, as an anode catalyst

support material for glucose electrooxidation has not been reported yet.

In this study,  $\text{PdIn/HAp}$  anode catalyst with varying atomic molar ratios was prepared by the  $\text{NaBH}_4$  reduction method and its electrocatalytic performance was investigated for the glucose electrooxidation reaction. XRD, XPS, BET, SEM-EDX, TEM, and ICP-MS methods were used to characterize  $\text{PdIn/HAp}$  electrocatalysts. The electrochemical performance of the synthesized catalysts was determined by electrochemical impedance spectroscopy (EIS), chronoamperometry (CA), and cyclic voltammetry (CV).

## Materials and methods

### Reagents

Calcium nitrate tetrahydrate ( $\text{Ca}(\text{NO}_3)_2 \cdot 4\text{H}_2\text{O}$ ), Indium (III) chloride ( $\text{InCl}_3$ ), Potassium tetrachloropalladate (II) ( $\text{K}_2\text{PdCl}_4$ ), di-ammonium hydrogen phosphate ( $(\text{NH}_4)_2\text{HPO}_4$ ), ammonia, and sodium borohydride ( $\text{NaBH}_4$ ) were purchased from Sigma-Aldrich and used for the synthesis of  $\text{PdIn/HAp}$  catalysts. All chemicals used for the preparation of  $\text{PdIn/HAp}$  are in analytical grade. Nafion 117 (5%), potassium hydroxide (KOH, 90%) and D-glucose ( $\text{C}_6\text{H}_{12}\text{O}_6$ , 98%) were utilized for electrochemical tests.

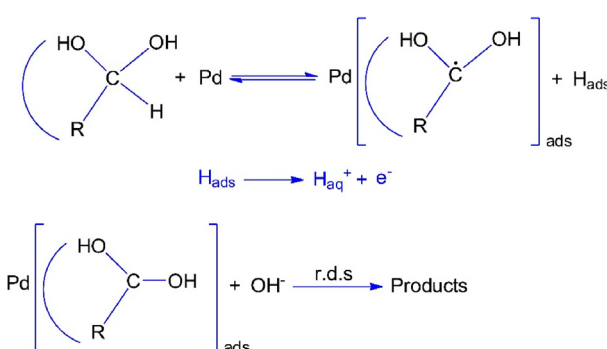
### Preparation of hydroxyapatite powder

The synthesis of Indium (III) chloride ( $\text{InCl}_3$ ) doped hydroxyapatite (HAp) powders were effectuated by a co-precipitation method. The reagents, di-ammonium hydrogen phosphate (S2) and calcium nitrate tetrahydrate (S1) were dissolved in DI to prepare the solutions with a certain molar ratio ( $\text{Ca}/\text{P} = 1.67$ ). Ammonia was added drop by drop into the S2 solution and continuously stirred for 1 h. After 24 h of aging, the final solution (S3) was filtered to obtain a wet cake. Afterward, the filtered Indium (III) chloride ( $\text{InCl}_3$ ) doped HAp was dried in an oven at  $200^\circ\text{C}$  to remove the excess water and ammonia. The sintering process for the resulting powders was applied at  $1100^\circ\text{C}$  in the air for 1 h. A schematic representation of HAp preparation is shown in Scheme 2.

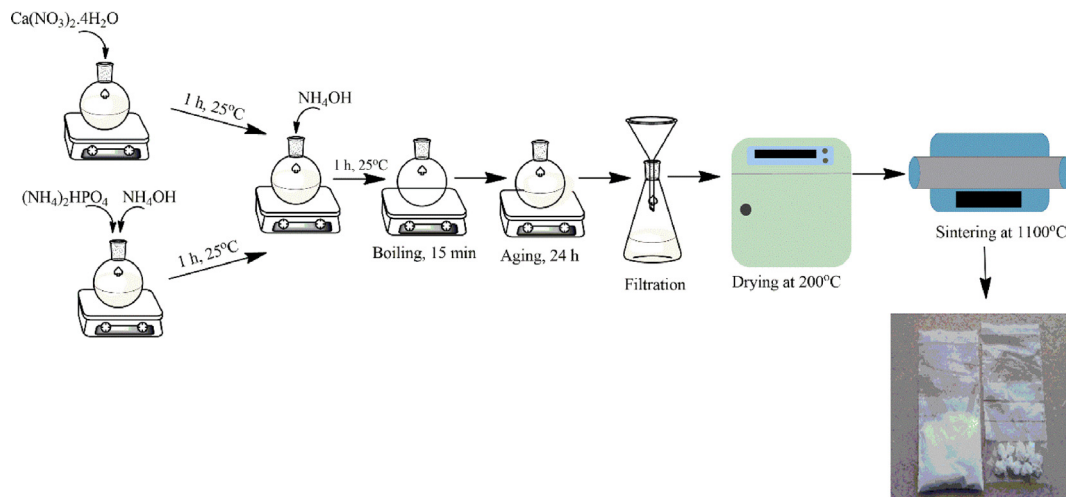
### Preparation and characterization of $\text{PdIn/HAp}$

10%  $\text{PdIn/HAp}$ s at varying metal compositions were prepared with the  $\text{NaBH}_4$  reduction method [66].  $\text{PdIn/HAp}$  catalysts were synthesized at  $\text{Pd:In}$  atomic molar ratios of 99:1, 90:10, 80:20, 70:30, 60:40, and 50:50. As reported in our previous study, metal salts containing Pd and In were stirred in distilled water, and 100 mg of HAp was put in the solution and stirred at room temperature for 60 min [67]. Metal salts were reduced by adding  $\text{NaBH}_4$  dropwise to the solution in a 1:15 M metal/ $\text{NaBH}_4$  ratio. The solution, which was stirred for an additional 30 min, was filtered, washed, and dried at  $85^\circ\text{C}$  for 12 h.

PANalytical Empyrean X-ray diffractometer with  $\text{Cu K}\alpha$  radiation ( $\lambda = 1.54056 \text{ \AA}$ ) was used to determine the crystal



**Scheme 1 – Mechanism of glucose electrooxidation on Pd catalyst.**



Scheme 2 – Synthesis procedure of HAp.

phases of the obtained catalysts. Hitachi HighTech HT7700 TEM device was used to observe the average particle size and particle distribution, and the TEM images were analyzed with ImageJ software. The Pd/In molar metal ratios of PdIn/HAp electrocatalysts were determined via the ICP-MS method with Agilent 7800 device.

#### Electrochemical evaluation

CHI-660E potentiostat with a conventional three electrodes system was utilized for the determination of glucose electro-oxidation performance of as-synthesized catalysts. Glassy carbon (GCE), Pt wire, and Ag/AgCl were used as working, counter, and reference electrodes, respectively. Specific activities of all catalysts in this study were normalized to the geometric area of the working electrode. All electrochemical experiments were performed in 1 M KOH + 0.5 M Glucose solution. For the preparation of the glassy carbon electrode, 5 mg of PdIn/HAp and 1 ml of Nafion 117 solution were ultrasonicated to obtain catalyst ink. 5 µl of catalyst ink was transferred to the surface of GCE and dried. The electrochemical activity of PdIn/HAps was investigated using CV

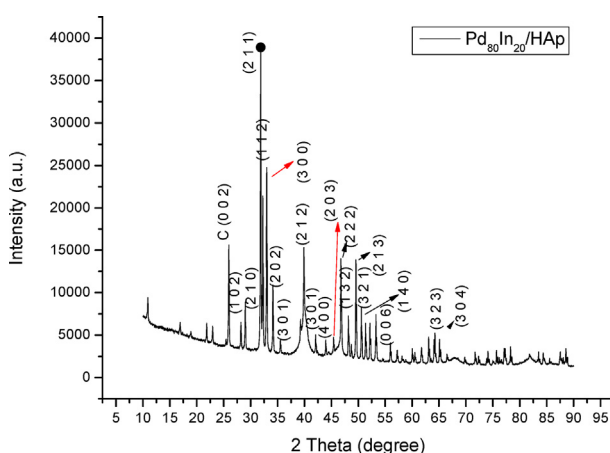
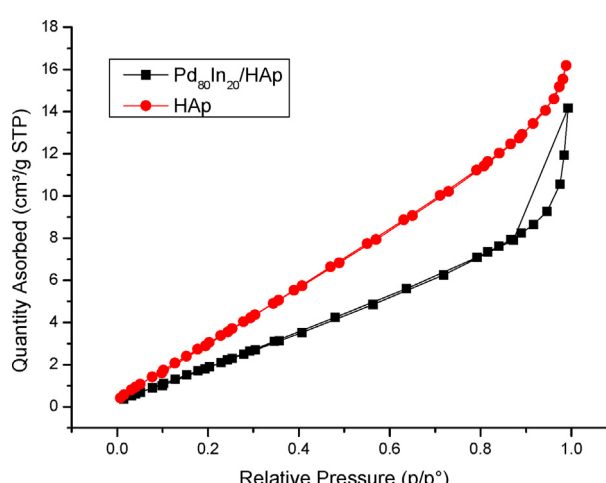
between the potential range of -0.23-1 V at 50 mV/s scan rate. The stability of the catalysts was specified with CA at 50 mV/s scan rate and 1 V potential. The electrocatalytic activity and charge transfer resistance of PdIn/HAps were determined from the EIS profile at 1 V potential.

## Results and discussion

#### Characterization of PdIn/HAp

The crystallinity of the synthesized catalysts was determined by the XRD method. The particle size distributions and average particle size of PdIn/HAp were analyzed by TEM. XPS and BET methods were used to determine surface oxidation property and N<sub>2</sub> adsorption-desorption behavior of PdIn/HAp. Also, the atomic molar ratios of PdIn/HAps were investigated by ICP-MS.

Fig. 1 displays the XRD pattern of Pd<sub>80</sub>In<sub>20</sub>/HAp. The observed diffraction peaks of HAp in the XRD pattern are highly compatible with JCPDS data No: 09–432, and HAp is predominantly in the hexagonal crystalline phase [68]. Also,

Fig. 1 – XRD pattern of Pd<sub>80</sub>In<sub>20</sub>/HAp.Fig. 2 – BET isotherms of HAp and Pd<sub>80</sub>In<sub>20</sub>/HAp.

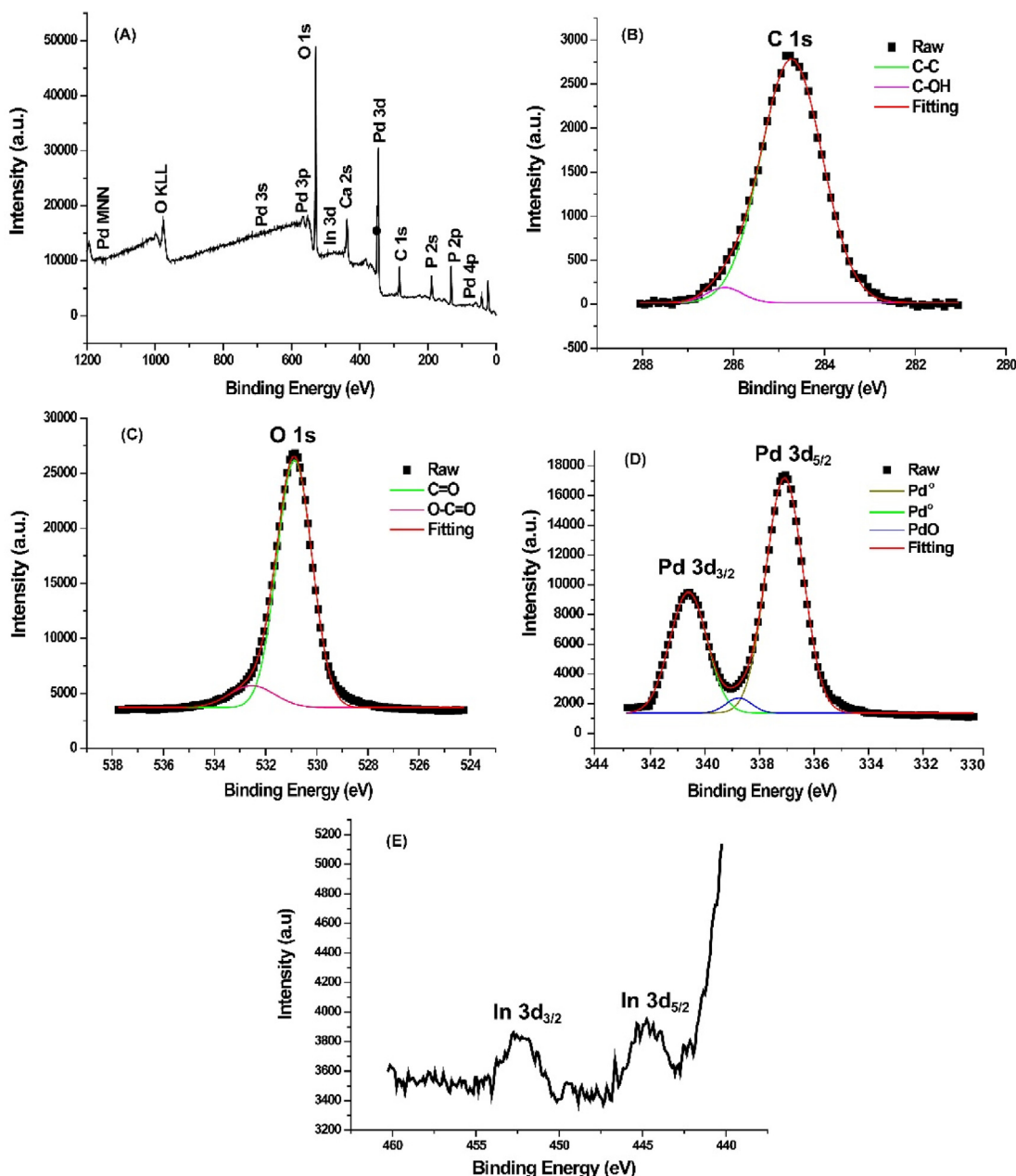
**Table 1 – Results obtained from N<sub>2</sub> adsorption-desorption isotherms.**

Electrocatalyst	S <sub>BET</sub> (m <sup>2</sup> /g)	Pore volume (cm <sup>3</sup> /g)	Pore size (nm)
HAp	9.54	0.0220	6.04
Pd <sub>80</sub> In <sub>20</sub> /HAp	14.0	0.0253	6.27

the XRD pattern of plain HAp is given in [Figure S1](#) and is used to label the diffraction peaks of Pd and In. The diffraction peaks of Pd distributed on the HAp were observed as shoulder peaks since they were located at similar 2θ angles to the diffraction peaks of the HAp. The shoulder peaks observed at 2θ angles of 40.0°, 46.9°, and 82.1° were attributed to Pd (1 1 1), Pd (2 0 0), and Pd (3 1 1) facets [69]. In addition, the diffraction

peak observed at 2θ of 39.2° is due to the In (1 1 1) peak [70]. The shifts observed in the characteristic diffraction peaks of face center cubic Pd (JCPDS card no. 05–0681) indicate that Pd is alloyed with In to form a new phase [71]. Moreover, the crystal size of Pd<sub>80</sub>In<sub>20</sub>/HAp was found to be 6.81 nm by the Scherer equation.

BET adsorption-desorption experiment was used to obtain the porosity and the surface area of HAp and PdIn/HAp. The parameters of pore structure and BET isotherms for HAp and Pd<sub>80</sub>In<sub>20</sub>/HAp were exhibited in [Fig. 2](#) and [Table 1](#). According to the UIPAC classification, plain HAp conforms to the type II isotherm, while the N<sub>2</sub> adsorption-desorption behavior of the Pd<sub>80</sub>In<sub>20</sub>/HAp catalyst could be explained by the type III isotherm ([Fig. 2](#)). The N<sub>2</sub> adsorption-desorption behaviors of HAp and Pd<sub>80</sub>In<sub>20</sub>/HAp catalysts were attributed to strong and

**Fig. 3 – a) General spectrum, b) C 1s, c) O 1s, d) Pd 3d, and In 3d core-level XPS spectra of Pd<sub>80</sub>In<sub>20</sub>/HAp.**

weak adsorbate-adsorbent interactions, respectively [72]. The increase in volume adsorbed at low relative pressures was attributed to the existence of micropores in the structure. In the BET isotherm of HAp, a second enhancement was observed after a relative pressure greater than 0.9, indicating the presence of macropores. For Pd<sub>80</sub>In<sub>20</sub>/HAp, the second enhancement was detected after 0.8 relative pressure. S<sub>BET</sub>

values of HAp and Pd<sub>80</sub>In<sub>20</sub>/HAp were found to be 9.54 and 14.0 m<sup>2</sup>/g, respectively (Table 1).

The surface electronic state of Pd<sub>80</sub>In<sub>20</sub>/HAp was examined by using XPS (Fig. 3). Peaks indicating the presence of Pd, In, Ca, P, and C was observed from the XPS general spectrum of the Pd<sub>80</sub>In<sub>20</sub>/HAp catalyst (Fig. 3a). Calibration of binding energies for spectra was performed according to C 1s peak at 284.6 eV.

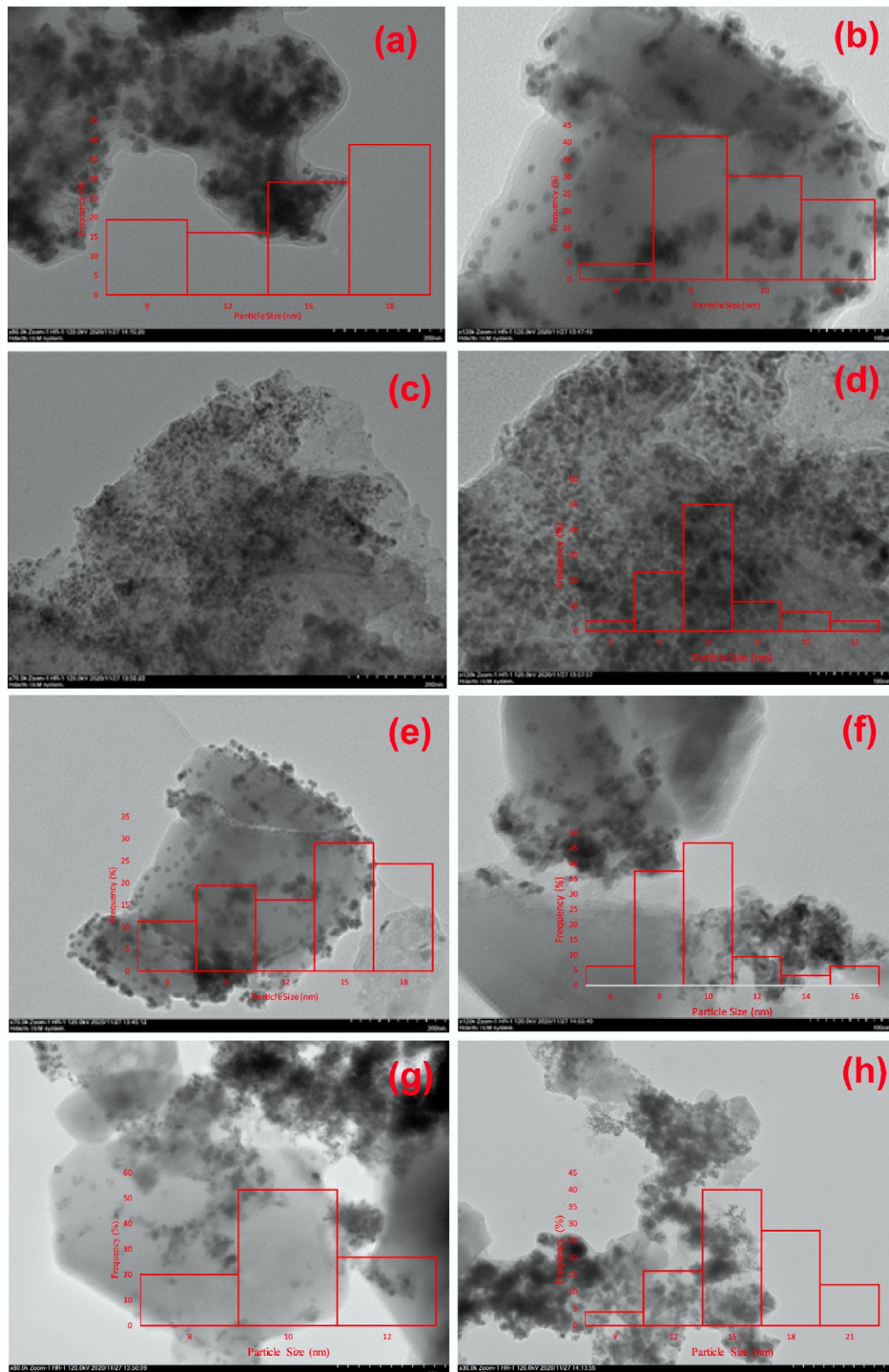


**Fig. 4 – TEM images of Pd<sub>80</sub>In<sub>20</sub>/HAp.**

The peaks detected at 284.6 and 286.1 eV binding energies were assigned to the presence of C–C and C–OH groups in the HAp structure (Fig. 3b) [73,74]. High-resolution XPS O 1s spectra obtained from Pd<sub>80</sub>In<sub>20</sub>/HAp displayed two deconvoluted peaks at binding energy of 530.8 and 532.4 eV associated with C=O and O–C=O [75] (Fig. 3c). Fig. 3d shows the high-resolution XPS spectrum of Pd. Pd 3d<sub>3/2</sub> and Pd 3d<sub>5/2</sub> were observed at binding energies of 340.6 and 337.3 eV and attributed to the presence of elemental Pd. Besides, the peak observed at 338.8 eV was assigned to the PdO form. It was concluded from the areas of the deconvoluted peaks that the Pd in the catalyst structure was predominantly in the form of Pd<sup>0</sup>. XPS spectrum of core-level In 3d is presented in Fig. 3e. The peaks observed at the binding energies of 452.3 and 444.7 eV correspond to In 3d<sub>3/2</sub> and In3d<sub>5/2</sub>, respectively. It has been concluded from XPS results that the metals used were successfully reduced to their elemental forms by the NaBH<sub>4</sub> method.

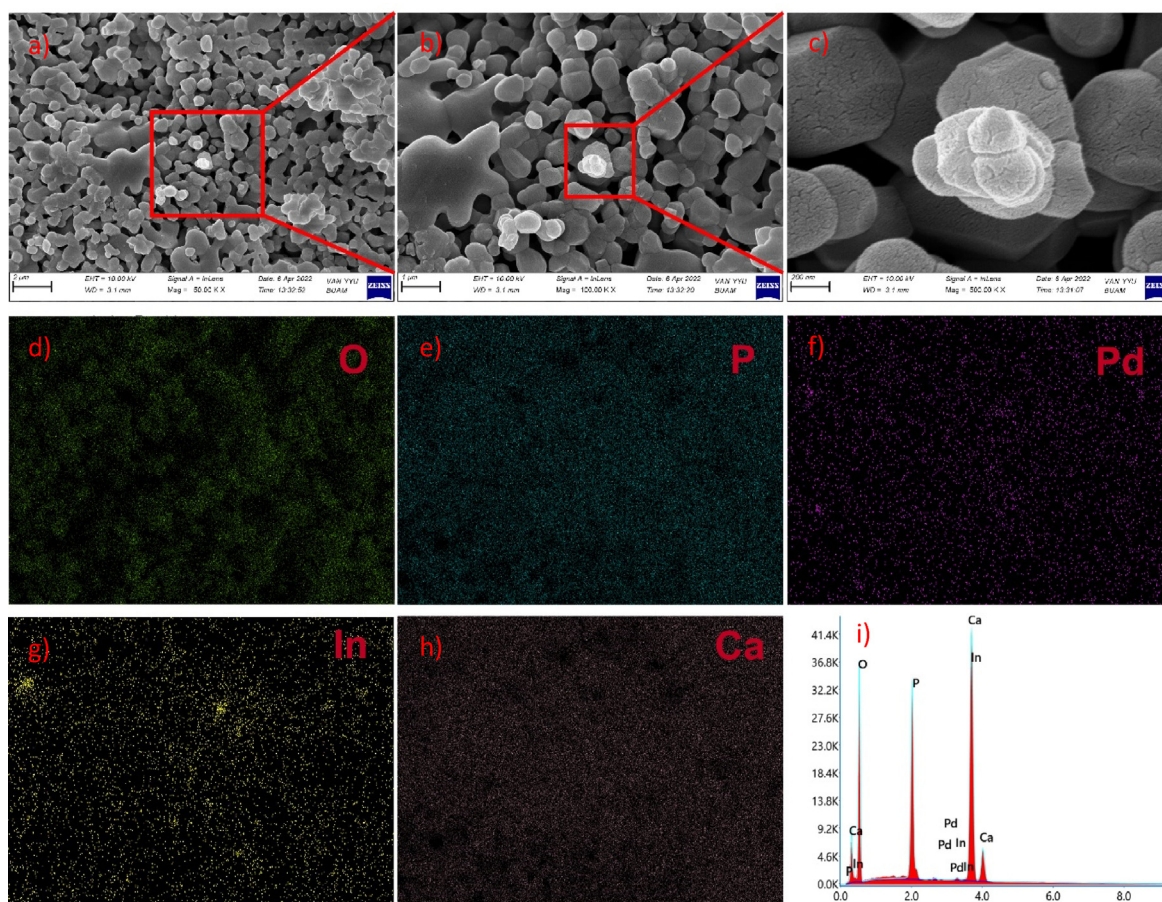
TEM images showing the distribution of nanoparticles on the HAp and corresponding particle size histograms were shown in Fig. 4. Although a severe agglomeration was observed in Fig. 4a and g, it was determined that the particles were more homogeneously distributed on the HAp in other TEM images. The observed agglomeration is due to the very rapid reduction of metal salts by NaBH<sub>4</sub>, which is used as a reductant. It is also evident from the particle size histograms that the particles are dispersed in a narrow size range. The average particle size was determined as 9.18 nm using ImageJ software.

Elemental distribution and morphology of Pd<sub>80</sub>In<sub>20</sub>/HAp were evaluated by performing SEM, EDX, and elemental mapping. Spherical nanoparticles were detected in the SEM image of Pd<sub>80</sub>In<sub>20</sub>/HAp (Fig. 5a–c). EDX results show that the Pd<sub>80</sub>In<sub>20</sub>/HAp catalyst contains P, Ca, O, Pd, and In in its structure (Fig. 5i). In addition, the distribution of O, P, and Ca in the structure of HAp was determined by elemental mapping analysis (Fig. 5d–h). The oxygen in the catalyst structure originates from the hydroxyl ions in HAp. Especially from Fig. 5f and g, it was observed that the Pd and In planes exhibited a uniform distribution on HAp support.

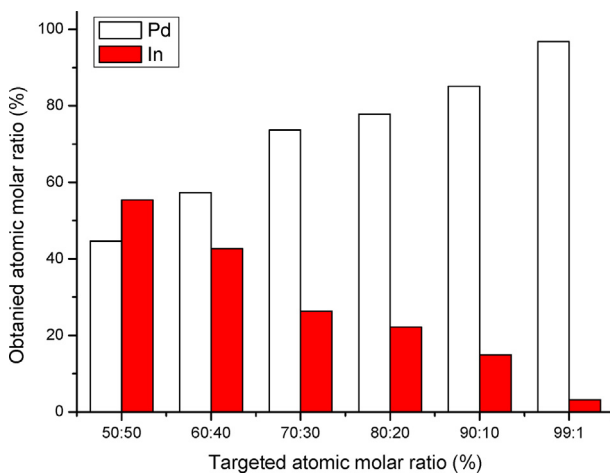
The atomic molar compositions of the PdIn/HAp catalysts were confirmed by ICP-MS and the results were given in Fig. 6. The molar Pd/In ratio of the Pd<sub>50</sub>In<sub>50</sub>/HAp, Pd<sub>60</sub>In<sub>40</sub>/HAp, Pd<sub>70</sub>In<sub>30</sub>/HAp, Pd<sub>80</sub>In<sub>20</sub>/HAp, Pd<sub>90</sub>In<sub>10</sub>/HAp, and Pd<sub>99</sub>In<sub>1</sub>/HAp catalysts were determined as 44.6/55.4, 57.3/42.7, 73.7/26.3, 77.8/22.2, 85.1/14.9, and 96.8/3.2, respectively. The fact that the metal ratios are almost the same as the targeted ratios indicates that the synthesis is successful in terms of obtained metallic molar ratios.

### Electrochemical evaluation

The electrocatalytic performance of the PdIn/HAp catalysts for glucose electrooxidation was determined in 1 M KOH+0.5 M Glucose electrolyte at 50 mV/s scan rate by EIS, CV, and CA. The electrocatalytic performances of PdIn/HAp were compared with HAp and Pd/HAp.

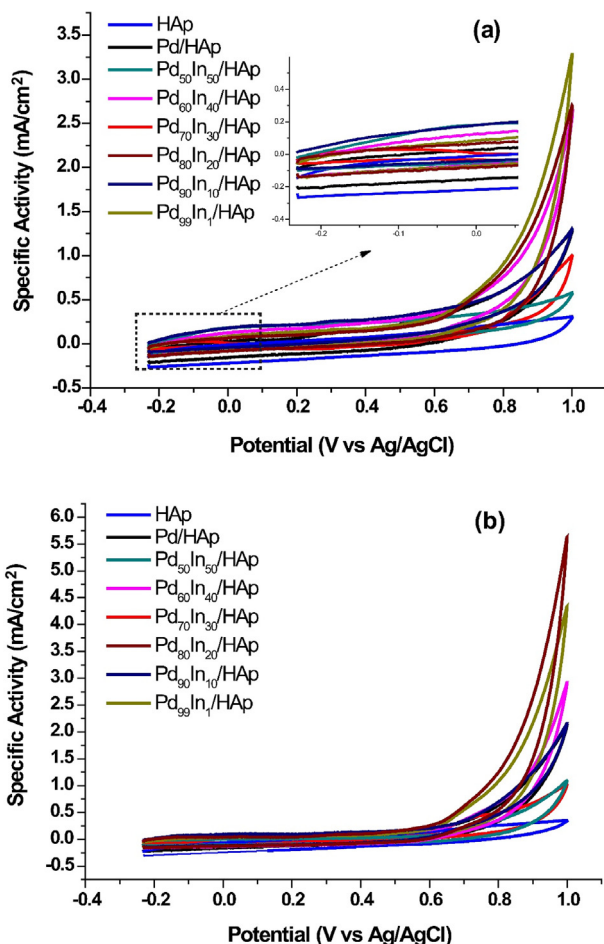


**Fig. 5 – SEM images, elemental mapping analysis, and EDX analysis of Pd<sub>80</sub>In<sub>20</sub>/HAp.**

**Fig. 6 – ICP-MS results of PdIn/HAp.****Glucose electrooxidation activity**

Cyclic voltammograms of PdIn/HAp catalysts at varying atomic molar ratios in 1 M KOH and 1 M KOH + 0.5 M Glucose solutions were presented in Fig. 7. Cyclic voltammograms of In/HAp catalyst in 1 M KOH and 1 M KOH + 0.5 M Glucose solution are shown in Figure S2. As can be seen from Figure S2, the specific activity of the In/HAp catalyst toward glucose electrooxidation is  $0.83 \text{ mA/cm}^2$ . It is seen from Fig. 7a that all catalysts except HAp have a hydrogen adsorption-desorption region at the potential range of  $-0.023 \text{ V}$ – $0.07 \text{ V}$ . In addition, a double layer region was observed in the potential range of  $0.016$ – $0.32 \text{ V}$  for the electrocatalysts other than  $\text{Pd}_{50}\text{In}_{50}/\text{HAp}$  and  $\text{Pd}_{60}\text{In}_{40}/\text{HAp}$  [76]. The peak observed at  $0.23 \text{ V}$  potential in the reverse scan for the voltammogram of the  $\text{Pd}_{70}\text{In}_{30}/\text{HAp}$  catalyst was attributed to PdO reduction [77]. From the areas of voltammograms recorded in KOH solution, it is clearly seen that the electrochemically active surface areas of  $\text{Pd}_{99}\text{In}_{1}/\text{HAp}$ ,  $\text{Pd}_{80}\text{In}_{20}/\text{HAp}$ , and  $\text{Pd}_{60}\text{In}_{40}/\text{HAp}$  electrocatalysts are higher than other electrocatalysts.

It is seen that the electrochemically active surface area of HAp increased with the addition of Pd (Fig. 7b). With the addition of Pd, the specific activity of HAp for glucose electrooxidation increased approximately 6 times. All synthesized anode catalysts were found to be active for glucose electrooxidation from the obtained specific activity values in 1 M KOH and 1 M KOH + 0.5 M Glucose solution (Table 2). Among the catalysts obtained by adding In to Pd/HAp, only the electrocatalytic activity of  $\text{Pd}_{60}\text{In}_{40}/\text{HAp}$ ,  $\text{Pd}_{80}\text{In}_{20}/\text{HAp}$ ,  $\text{Pd}_{90}\text{In}_{10}/\text{HAp}$ , and  $\text{Pd}_{99}\text{In}_{1}/\text{HAp}$  catalysts increased. The deviation of the distance between the d band center of Pd and the Fermi level from its optimum value for glucose electrooxidation is one of the main reasons for the decrease in the specific activities of other catalysts [69].  $\text{Pd}_{80}\text{In}_{20}/\text{HAp}$  displayed the highest electrocatalytic activity with a specific activity of  $5.64 \text{ mA/cm}^2$  for glucose electrooxidation compared to that of other PdIn/Haps. The relatively low specific activities of  $\text{Pd}_{70}\text{In}_{30}/\text{HAp}$  and  $\text{Pd}_{50}\text{In}_{50}/\text{HAp}$  ( $1.09$  and  $1.02 \text{ mA/cm}^2$ ) are due to the oxidation of carbonaceous compounds at a potential of about  $0 \text{ V}$ . With the addition of In, the onset potential of Pd-based catalysts shifted to

**Fig. 7 – CV curves of PdIn/HAp catalysts in a) 1 M KOH and b) 1 M KOH + 0.5 M Glucose.**

negative potentials compared to that of Pd/HAp, indicating that the poisoning severity of PdIn alloy catalysts for glucose electrooxidation decreased due to the synergism between Pd and In Ref. [78].

**Electrochemical stability**

Chronoamperometric curves of HAp, Pd/HAp, and  $\text{Pd}_{80}\text{In}_{20}/\text{HAp}$  in 1 M KOH + 0.5 M Glucose solution at a scan rate of 50 mV/s were given in Fig. 8. The current density of the  $\text{Pd}_{80}\text{In}_{20}/\text{HAp}$  catalyst dropped sharply from  $2.76 \text{ mA/cm}^2$  to  $1.96 \text{ mA/cm}^2$  in the first 25 s. The initial current drop in the first 25 s for HAp and Pd/HAp were found to be  $2.29$  and  $1.14 \text{ mA/cm}^2$ , respectively, and the sharp decrease in current density was assigned to carbonaceous compounds deposited on the catalyst surface. The percentage current loss after 1000 s for HAp, Pd/HAp, and  $\text{Pd}_{80}\text{In}_{20}/\text{HAp}$  was determined as 94.9%, 62.6%, and 49.6, respectively. From Fig. 8b, it is clear that the  $\text{Pd}_{80}\text{In}_{20}/\text{HAp}$  catalyst has the longest stability for 1000 s compared to these of Pd/HAp and HAp. As shown in Figure S3, the glucose diffusion coefficient for HAp, Pd/HAp, and  $\text{Pd}_{80}\text{In}_{20}/\text{HAp}$  were determined with the slope of the linear plot of  $I$  vs.  $t^{-1/2}$ . Cottrell equation was used to obtain the diffusion coefficient of the glucose:

**Table 2 – Electrochemical performance of PdIn/HAp.**

Catalysts	Specific Activity in 1 M KOH	Onset Potential in 1 M KOH + 0.5 M Glucose	Specific Activity in 1 M KOH + 0.5 M Glucose
HAp	0.31	–	0.35
In/HAp	0.46	0.35	0.83
Pd/HAp	1.28	0.75	2.12
Pd <sub>50</sub> In <sub>50</sub> /HAp	0.58	0.67	1.02
Pd <sub>60</sub> In <sub>40</sub> /HAp	2.59	0.65	2.92
Pd <sub>70</sub> In <sub>30</sub> /HAp	1.00	0.69	1.09
Pd <sub>80</sub> In <sub>20</sub> /HAp	3.28	0.62	5.64
Pd <sub>90</sub> In <sub>10</sub> /HAp	1.30	0.67	2.16
Pd <sub>99</sub> In <sub>1</sub> /HAp	2.70	0.63	4.34

$$i(t) = \frac{nFACD^{1/2}}{t^{1/2}\pi^{\frac{1}{2}}} = Kt^{-1/2} \quad (4)$$

where C, D, and A represent the concentration of glucose, diffusion coefficient, and real surface area. Diffusion coefficient of the glucose for HAp/GCE, Pd/HAp/GCE, and PdIn/HAp/GCE was calculated to be  $7.81 \times 10^{-10}$ ,  $1.29 \times 10^{-9}$ , and  $5.94 \times 10^{-10} \text{ cm}^2 \text{ s}^{-1}$ , respectively.

#### Impedance patterns for glucose electrooxidation

Fig. 9a shows the EIS profiles of Pd<sub>80</sub>In<sub>20</sub>/HAp, Pd/HAp, and HAp materials in 1 M KOH + 0.5 M Glucose solution at 1 V

potential. The decrease in the diameter of the EIS curves indicates decreased charge transfer resistance and increased electrocatalytic activity. Accordingly, Pd<sub>80</sub>In<sub>20</sub>/HAp showed higher electrocatalytic activity for glucose electrooxidation than other catalysts, and the EIS results are in harmony with the CV and CA results. Electrochemical tests show that Pd<sub>80</sub>In<sub>20</sub>/HAp has higher specific activity and stability for glucose electrooxidation than other anode catalysts. The performance of Pd<sub>80</sub>In<sub>20</sub>/HAp is attributed to the alteration of its electronic properties by modifying the surface of Pd with In and the optimum value of the distance between the Fermi level and the d band center of Pd. The fitted EIS profile of the Pd<sub>80</sub>In<sub>20</sub>/HAp was shown in Fig. 9b. R, W, and Q in the equivalent resistance model represent the resistance, Warburg element, and the constant phase element, respectively. Obtaining good fitting shows that the electrooxidation process on Pd<sub>80</sub>In<sub>20</sub>/HAp could be sensibly explained by the proposed equivalent circle model. In the proposed model, R<sub>1</sub> and R<sub>2</sub> are attributed to the resistance of the solution, while R<sub>3</sub> of 3.380 Ω cm<sup>2</sup> represents the charge transfer resistance.

The effect of scan rates on the electrooxidation of Pd<sub>80</sub>In<sub>20</sub>/HAp catalyst in 1 M KOH and 0.5 M Glucose solution is shown in Fig. 10a. It was determined from Fig. 10a that the peak current for glucose electrooxidation increased as the scan rates increased. Fig. 10b shows a linear relationship between scan rates and peak current for glucose electrooxidation on PdIn/HAp, indicating glucose is transported from the bulk

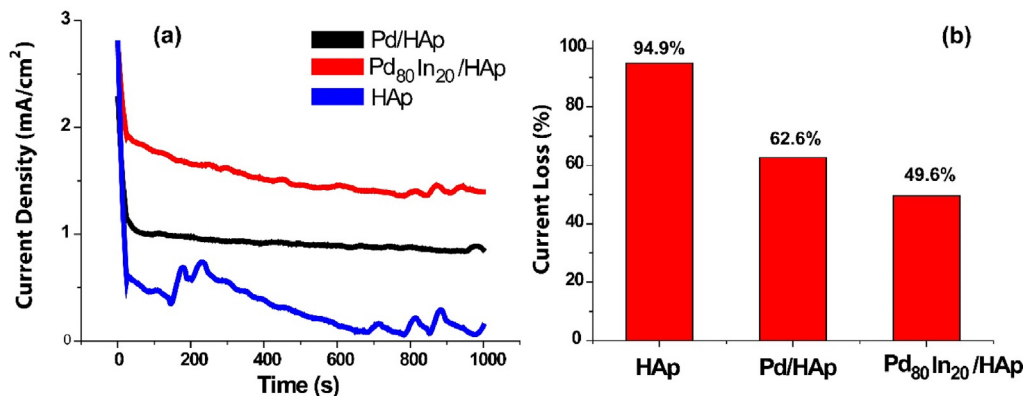


Fig. 8 – a) Chronoamperometric curves and b) current loss after 1000 s for Pd<sub>80</sub>In<sub>20</sub>/HAp in 1 M KOH + 0.5 M Glucose.

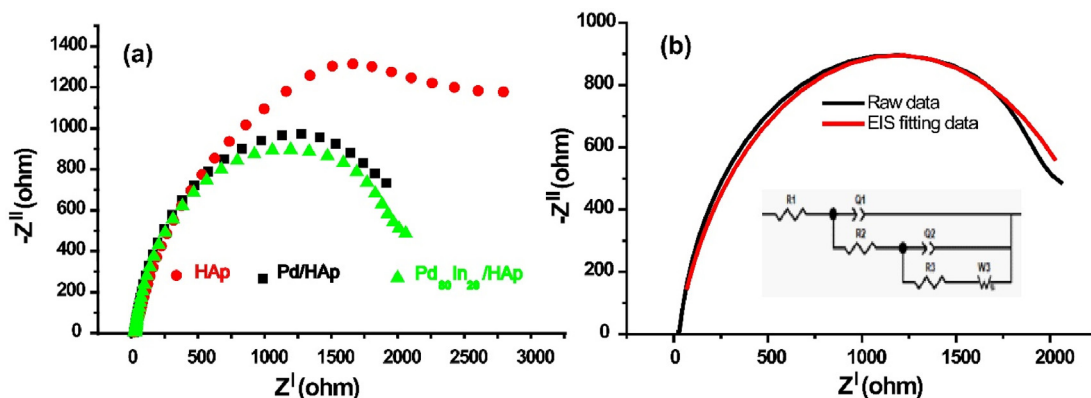
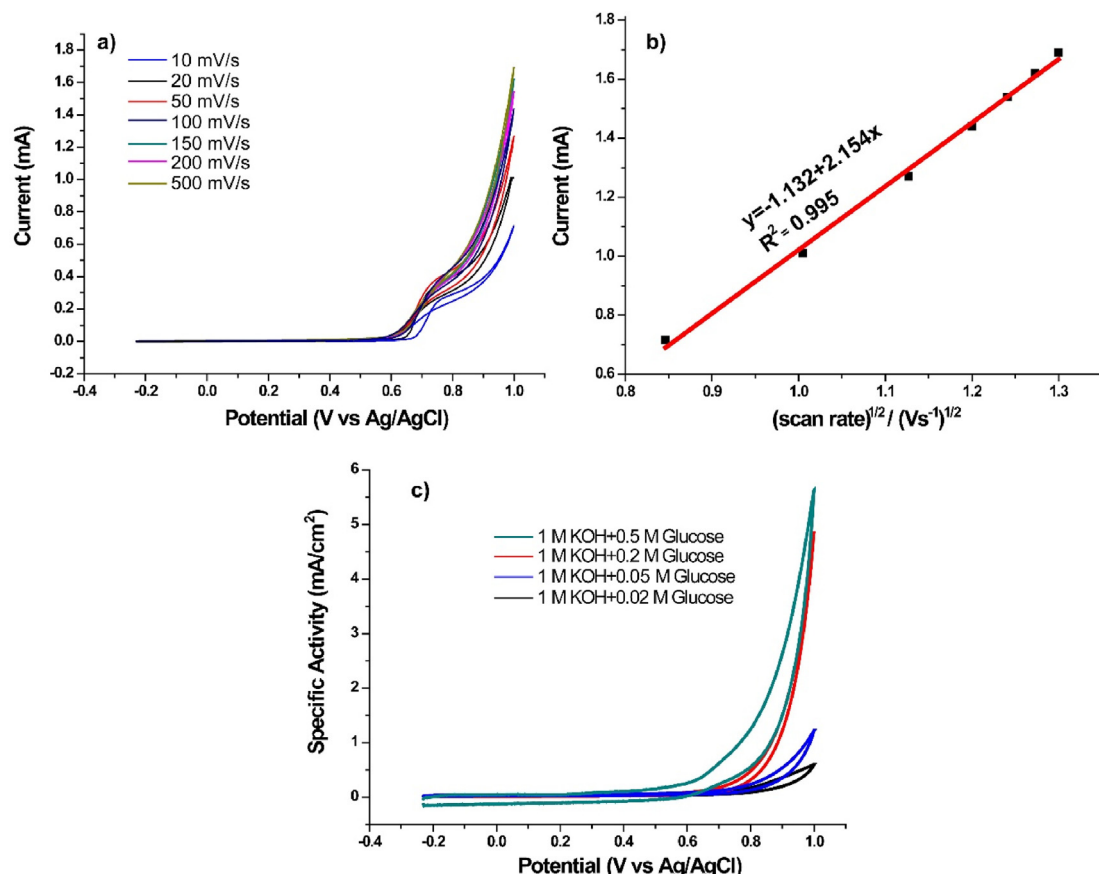


Fig. 9 – a) EIS profiles of PdIn/HAp, Pd/HAp, and HAp, and b) equivalent circuit model for Pd<sub>80</sub>In<sub>20</sub>/HAp for glucose electrooxidation.



**Fig. 10 – (a)** CV of the PdIn/HAp in 1 M KOH + 0.5 M glucose at varying scan rates, **(b)** current vs.  $(\text{scan rate})^{1/2}$ , and **(c)** 1 M KOH + 0.02–0.5 M glucose.

solution to the PdIn/HAp modified GCE surface predominantly by mass transfer [29]. The effect of glucose concentration on glucose electrooxidation with Pd<sub>80</sub>In<sub>20</sub>/HAp is shown in Fig. 10c. The specific activities were determined as 0.60, 1.22, 4.87 and 5.64 mA/cm<sup>2</sup> for 0.02, 0.05, 0.2 and 0.5 M glucose concentrations in 1 M KOH solution, respectively. The

increase in specific activity with increasing glucose concentration was attributed to the presence of sufficient OH<sup>-</sup> group adsorption on active sites of PdIn/HAp [79].

In the literature, the activities of various materials toward the glucose electrooxidation reaction were generally reported for sensor applications. There is limited literature on the fuel

**Table 3 – Literature on anode catalyst for glucose electrooxidation.**

Anode catalyst	Solution (C <sub>KOH</sub> or NaOH/Glucose)	Scan rate (mV/s)	Specific activity (mA/cm <sup>2</sup> )	Mass activity (mA/mg)	Onset potential (V)	References
Pt/Pd/p-1,8-DAN	0.10 M/0.025 M	50	0.051	–	-0.28	[80]
AgPt@C	1 M/5 mM	50	0.025	–	0.15	[81]
Pd–Ce <sub>2</sub> O <sub>3</sub> /ITO	0.5 M/0.5 M	50	8.125	–	0.101	[82]
Mg <sub>65</sub> Bi <sub>35</sub>	0.5 M/0.5 M	50	8.04	125	0.513	[43]
Benzothiophene derivative	1 M/0.5 M	50	0.729	3.345	-0.19	[83]
Pd <sub>90</sub> In <sub>10</sub> /CNT	1 M/0.5 M	50	0.98	161.15	-0.319	[52]
N doped-G/ITO	1 M/0.5 M	50	9.12	–	-0.22	[84]
Pd <sub>3</sub> Cu–B/C	0.1 M/0.5 M	100	–	105	–	[29]
Graphene/Ni–Fe	0.2 M/0.01 M	50	ca. 0.5	–	0.3	[50]
G/ITO	1 M/0.5 M	50	6.58	–	-0.24	[69]
Pt–Ni–Cu/GCE	0.1 M/0.01 M	100	0.96	–	ca -0.5	[51]
Indole-based organic catalyst	1 M/0.5 M	50	0.52	2.45	0.57	[85]
CoO <sub>x</sub> @CNF	0.1 M/0.05 M	50	ca 6	–	–	[86]
Ru/CNT	1 M/0.5 M	50	1.86	160.6	–	[38]
Ni–Cu/GC	0.5 M/0.05 M	100	–	409	ca 0.2	[45]
Pd <sub>80</sub> In <sub>20</sub> /HAp	1 M + 0.5 M	50	5.64	159.4	0.62	In this study

cell, which requires electrochemical measurements with higher glucose and supporting electrolyte concentrations compared to sensor applications. The electrochemical performances of the materials prepared as anode catalysts for DGFCs in recent years were summarized in Table 3. Elkholy et al. reported the specific activity for glucose electrooxidation on Pd–Ce<sub>2</sub>O<sub>3</sub>/ITO as 8.125 mA/cm<sup>2</sup> and emphasized that Ce<sub>2</sub>O<sub>3</sub> had a lowering effect on the charge transfer resistance [82]. On the other hand, Shi et al. reported the specific activity of Mg–Bi alloy catalyst as 8.04 mA/cm<sup>2</sup> under similar conditions [43]. In our study, the specific activity of glucose electrooxidation with Pd<sub>80</sub>In<sub>20</sub>/HAp electrocatalyst was found to be 5.64 mA/cm<sup>2</sup>. The specific activity of Pd<sub>80</sub>In<sub>20</sub>/HAp for glucose electrooxidation can compete with the activity values obtained under similar conditions in the literature. Er et al., reported the specific activity of CNT-supported PdIn alloy catalyst for glucose electrooxidation as 0.98 mA/cm<sup>2</sup> [52]. The electrocatalytic performance of Pd<sub>80</sub>In<sub>20</sub>/HAp catalyst is 5.8 times higher than Pd<sub>90</sub>In<sub>10</sub>/CNT, indicating that HAp could be a good alternative to CNT. The positive contribution of HAp to the electrocatalytic activity is attributed to the fact that Ca and phosphate in its structure create isolated Pd regions and enable the third-body effect [87]. In addition, it was concluded that the hydroxyl-rich structure of HAp caused the separation of CO species from the catalyst surface and increased the electrocatalytic activity for glucose electrooxidation by bifunctional effect.

## Conclusions

PdIn/HAs were successfully synthesized by precipitation and NaBH<sub>4</sub> reduction method toward glucose electrooxidation. The morphological and chemical structure of PdIn/HAp were investigated by using TEM, XRD, and ICP-MS. The average particle size and crystal size of the PdIn nanoparticles are found to be 9.18 nm and 6.81 nm, respectively. Among the PdIn/HAs at different metal compositions, the Pd<sub>80</sub>In<sub>20</sub>/HAp catalyst exhibited the highest electrocatalytic activity for glucose electrooxidation with a specific activity of 5.64 mA/cm<sup>2</sup>. The percentage current loss after 1000 s for HAp, Pd/HAp, and Pd<sub>80</sub>In<sub>20</sub>/HAp was determined as 94.9%, 62.6%, and 49.6, respectively. The Pd<sub>80</sub>In<sub>20</sub>/HAp catalyst has long-term stability at higher activity than Pd/HAp and HAp. The charge transfer resistance of the Pd<sub>80</sub>In<sub>20</sub>/HAp catalyst was found to be 3380 Ω/cm<sup>2</sup>. The charge transfer resistance of Pd<sub>80</sub>In<sub>20</sub>/HAp is lower than HAp and Pd/HAp. Thanks to the hydroxyl ions in the HAp structure, increases the CO tolerance of the catalyst system. It is predicted that HAp will be used more widely as a catalyst support material, as it reduces the severity of CO poisoning, which is an important handicap for the oxidation of carbon-containing fuels namely glucose, ethylene glycol, formic acid, methanol, and ethanol.

## Declaration of competing interest

The authors declare that they have no known competing financial interests or personal relationships that could have appeared to influence the work reported in this paper.

## Appendix A. Supplementary data

Supplementary data to this article can be found online at <https://doi.org/10.1016/j.ijhydene.2022.06.314>.

## REFERENCES

- [1] Cali A, Yağızatlı Y, Sahin A, Ar İ. Highly durable phosphonated graphene oxide doped polyvinylidene fluoride (PVDF) composite membranes. *Int J Hydrogen Energy* 2020;45:35171–9.
- [2] Liu Z, Kendall K, Yan X. China progress on renewable energy vehicles: fuel cells, hydrogen and battery hybrid vehicles. *Energies* 2019;12:54.
- [3] Keller A, Karpukhin K, Kolbasov A, Kozlov V. Analysis of hydrogen use as an energy carrier in transport. IOP conference series: Materials Science and Engineering: IOP Publishing; 2021. p.012087.
- [4] Gouda MH, Konsowa AH, Farag HA, Elessawy NA, Tamer TM, Eldin MSM. Development novel eco-friendly proton exchange membranes doped with nano sulfated zirconia for direct methanol fuel cells. *J Polym Res* 2021;28:1–10.
- [5] Sharma R, Arya BD, Malik N. Proton exchange membrane fuel cells: An overview. *World Wide J Multidiscip Res Dev* 2015;1(2):18–22.
- [6] Yagizatlı Y, Ulas B, Cali A, Sahin A, Ar I. Improved fuel cell properties of Nano-TiO<sub>2</sub> doped Poly(Vinylidene fluoride) and phosphonated Poly(Vinyl alcohol) composite blend membranes for PEM fuel cells. *Int J Hydrogen Energy* 2020;45:35130–8.
- [7] Wang W, Wang Y, Liu S, Yahia M, Dong Y, Lei Z. Carbon-supported phosphatized CuNi nanoparticle catalysts for hydrazine electrooxidation. *Int J Hydrogen Energy* 2019;44:10637–45.
- [8] Wang H, Ding J, Kannan P, Ji S. Cobalt nanoparticles intercalated nitrogen-doped mesoporous carbon nanosheet network as potential catalyst for electro-oxidation of hydrazine. *Int J Hydrogen Energy* 2020;45:19344–56.
- [9] Eshghi A, Sabzehei M. Platinum–Iron nanoparticles supported on reduced graphene oxide as an improved catalyst for methanol electro oxidation. *Int J Hydrogen Energy* 2018;43:6107–16.
- [10] Askari MB, Rozati SM, Salarizadeh P, Saeidfirozeh H, Di Bartolomeo A. A remarkable three-component RuO<sub>2</sub>–MnCo<sub>2</sub>O<sub>4</sub>/rGO nanocatalyst towards methanol electrooxidation. *Int J Hydrogen Energy* 2021;46:36792–800.
- [11] Caglar A, Kivrak H. Highly active carbon nanotube supported PdAu alloy catalysts for ethanol electrooxidation in alkaline environment. *Int J Hydrogen Energy* 2019;44:11734–43.
- [12] Mostashari SM, Dehkharghani RA, Afshar-Taromi F, Farsadrooh M. A straightforward one-pot synthesis of Pd–Ag supported on activated carbon as a robust catalyst toward ethanol electrooxidation. *Int J Hydrogen Energy* 2021;46:9406–16.
- [13] Ashok A, Kumar A. Ag/Co<sub>3</sub>O<sub>4</sub> as an effective catalyst for glycerol electro-oxidation in alkaline medium. *Int J Hydrogen Energy* 2021;46:4788–97.
- [14] Ghaith ME, El-Nagar GA, Abd El-Moghny MG, Alalawy HH, El-Shakre ME, El-Deab MS. Electrocatalysis by design: enhanced electro-oxidation of glycerol at NiOx nanoparticle modified 3D porous carbon felts. *Int J Hydrogen Energy* 2020;45:9658–68.
- [15] Santos AO, Silva JCM, Antoniassi RM, Ponzio EA, Alves OC. The formate electrooxidation on Pt/C and PtSnO<sub>2</sub>/C nanoparticles in alkaline media: the effect of morphology

- and SnO<sub>2</sub> on the platinum catalytic activity. *Int J Hydrogen Energy* 2020;45:33895–905.
- [16] Wang M, Lian T, Wang J, Cheng X, Zhao J, Song C, Wang L, Xi J. In-situ deposition and subsequent growth of Pd on SnO<sub>2</sub> as catalysts for formate oxidation with excellent Pd utilization and anti-poisoning performance. *Int J Hydrogen Energy* 2019;44:21518–26.
- [17] Chowdhury SR, Maiyalagan T. Enhanced electro-catalytic activity of nitrogen-doped reduced graphene oxide supported PdCu nanoparticles for formic acid electro-oxidation. *Int J Hydrogen Energy* 2019;44:14808–19.
- [18] He N, Gong Y, Yang Y, Wang Y, Qin C, Wang R, Liu J, Qi T. An effective Pd@ Ni-B/C anode catalyst for electro-oxidation of formic acid. *Int J Hydrogen Energy* 2018;43:3216–22.
- [19] Cai K, Wang C, Pu W, Gao Y, Mao Z. Investigation of anode flow field for direct dimethyl ether fuel cell. *Int J Hydrogen Energy* 2012;37:Journal:12605–8.
- [20] Caglar A, Kivrak H, Aktas N. The effect of titanium dioxide-supported CdSe photocatalysts enhanced for photocatalytic glucose electrooxidation under UV illumination. *Int J Hydrogen Energy* 2022;47:21130–45.
- [21] Kaya S, Ulas B, Duzenli D, Onal I, Er OF, Yilmaz Y, Tezsevin I, Kivrak H. Glucose electrooxidation modelling studies on carbon nanotube supported Pd catalyst with response surface methodology and density functional theory. *J Phys Chem Solid* 2022;168:110810.
- [22] Yavari Z, Meshginkhoud A, Molae Barjahri R, Kerman K, Noroozifar M. CH<sub>3</sub>OH electrooxidation by nanosized Pd loaded on porous LaMnO<sub>3</sub>. *Mater Today Chem* 2021;19:100398.
- [23] Kaedi F, Yavari Z, Abbasian AR, Kerman K, Noroozifar M. Nano-assembly Pd anchoring in the non-stoichiometric spongy zinc ferrite to catalyze the electro-oxidation of C1 organic compounds. *Ceram Int* 2020;46:25741–9.
- [24] Yagizatli Y, Ülas B, Sahin A, Ar I. Investigation of sulfonation reaction kinetics and effect of sulfonation degree on membrane characteristics for PEMFC performance. *Ionics* 2022;28:2323–36.
- [25] Beaucamp A, Culebras M, Collins MN. Sustainable mesoporous carbon nanostructures derived from lignin for early detection of glucose. *Green Chem* 2021;23:5696–705.
- [26] Huynh TTK, Tran TQN, Yoon HH, Kim W-J, Kim IT. AgNi@ZnO nanorods grown on graphene as an anodic catalyst for direct glucose fuel cells. *Kor J Chem Eng* 2019;36:1193–200.
- [27] Tsang C-HA, Hui K, Hui K. Electrooxidation of glucose by binder-free bimetallic Pd<sub>1</sub>Ptx/graphene aerogel/nickel foam composite electrodes with low metal loading in basic medium. *Electrochim Acta* 2017;258:371–9.
- [28] Zhiani M, Abedini A, Majidi S. Comparison of electro-catalytic activity of Fe-Ni-Co/C and Pd/C nanoparticles for glucose electro-oxidation in alkaline half-cell and direct glucose fuel cell. *Electrocatalysis* 2018;9:735–43.
- [29] Chai D, Zhang X, Chan SH, Li G. Facile aqueous phase synthesis of Pd<sub>3</sub>Cu–B/C catalyst for enhanced glucose electrooxidation. *J Taiwan Inst Chem Eng* 2019;95:139–46.
- [30] Mello GA, Chequepán W, Briega-Martos V, Feliu JM. Glucose electro-oxidation on Pt (100) in phosphate buffer solution (pH 7): a mechanistic study. *Electrochim Acta* 2020;354:136765.
- [31] Elahi MY, Heli H, Bathaie S, Mousavi M. Electrocatalytic oxidation of glucose at a Ni-curcumin modified glassy carbon electrode. *J Solid State Electrochem* 2007;11:273–82.
- [32] Basu D, Sood S, Basu S. Performance comparison of Pt–Au/C and Pt–Bi/C anode catalysts in batch and continuous direct glucose alkaline fuel cell. *Chem Eng J* 2013;228:867–70.
- [33] Yan L, Brouzgou A, Meng Y, Xiao M, Tsikaratas P, Song S. Efficient and poison-tolerant PdxAuy/C binary electrocatalysts for glucose electrooxidation in alkaline medium. *Appl Catal B Environ* 2014;150–151:268–74.
- [34] Chai D, Wang W, Wang F, Kang Y, Yang Y, Lei Z. A facile precipitation procedure for synthesis of binary Sn-Co oxide promoting Pd catalyst towards glucose electrooxidation. *Electrochim Acta* 2016;189:295–302.
- [35] Wang T-P, Hong B-D, Lin Y-M, Lee C-L. Catalysis of the D-glucose oxidation reaction using octahedral, rhombic dodecahedral, and cubic Pd@ Pt core-shell nanoparticles. *Appl Catal B Environ* 2020;260:118140.
- [36] Cao M, Cao H, Meng W, Wang Q, Bi Y, Liang X, Yang H, Zhang L, Lang M-F, Sun J. Nickel-copper oxide nanoflowers for highly efficient glucose electrooxidation. *Int J Hydrogen Energy* 2021;46:28527–36.
- [37] Awad M, Al-Hazemi ME, Al-thagafi ZT. Enhanced electrocatalytic oxidation of glucose on nickel oxides/graphene nanoparticles modified glassy carbon electrode. *Int J Electrochem Sci* 2022;17:2.
- [38] Er OF, Kivrak H. Highly active carbon nanotube supported iridium, copper, ruthenium catalysts for glucose electrooxidation. *Energy Storage* 2021;3:e271.
- [39] Kaya S, Ulas B, Er OF, Yilmaz Y, Kivrak H. Optimization of electrode preparation conditions for enhanced glucose electrooxidation on Pt/CNT by response surface methodology. *J Electron Mater* 2022;51:2971–81.
- [40] Awad M, Al-Hazemi ME, Al-thagafi ZT. Glucose electrooxidation at nickel nanoparticles modified glassy carbon electrode: tolerance to poisoning. *Int J Electrochem Sci* 2022;17:2.
- [41] Neto NFA, de Jesus Pereira AL, Leite DMG, da Silva JHD, da Silva Pelissari MR. Evaluation of ITO/TiO<sub>2</sub>/Co<sub>3</sub>O<sub>4</sub> as a non-enzymatic heterojunction electrode to glucose electrooxidation. *Ionics* 2021;27:1597–609.
- [42] Mo G, Zheng X, Ye N, Ruan Z. Nitrogen-doped carbon dodecahedron embedded with cobalt nanoparticles for the direct electro-oxidation of glucose and efficient nonenzymatic glucose sensing. *Talanta* 2021;225:121954.
- [43] Shi H, Tang C, Wang Z, Zhang Z, Liu W, Ding Y, Shen X. Nanoporous bismuth electrocatalyst with high performance for glucose oxidation application. *Int J Hydrogen Energy* 2021;46:4055–64.
- [44] Er ÖF, Ulas B, Kivrak HD. Remarkable bismuth-gold alloy decorated on MWCNT for glucose electrooxidation: the effect of bismuth promotion and optimization via response surface methodology. *J Turk J Chem* 2021;45:1173–88.
- [45] Abuzaid MM, Asal YM, Mohammad AM, Al-Akraa IM. Enhanced glucose electrooxidation at Ni-Cu binary oxide nanocatalyst. *Int J Electrochem Sci* 2020;15:2449–57.
- [46] Neha N, Kouamé BSR, Rafaideen T, Baranton S, Coutanceau C. Remarkably efficient carbon-supported nanostructured platinum-bismuth catalysts for the selective electrooxidation of glucose and methyl-glucoside. *Electrocatalysis* 2021;12:1–14.
- [47] Dong G, Lu Q, Jiang H, Li C, Gong Y, Zhang H, Li W. Electrocatalytic glucose oxidation at coral-like Pd/C<sub>3</sub>N<sub>4</sub>-C nanocomposites in alkaline media. *Catalysts* 2020;10:440.
- [48] Ahmad YH, Mohamed AT, El-Shafei A, Al-Qaradawi SY, Aljaber AS. Facile one-step synthesis of supportless porous AuPtPd nanocrystals as high performance electrocatalyst for glucose oxidation reaction. *Int J Hydrogen Energy* 2020;45:19163–73.
- [49] Yu B, Liu Y, Miao Y. Nanorods of Bi–Co–S for electrocatalysis of glucose oxidation and hydrogen evolution. *J Electrochem Energy Convers Storage* 2020;17:031005.
- [50] Eshghi A, Kheirmand M. Graphene/Ni–Fe layered double hydroxide nano composites as advanced electrode materials for glucose electro oxidation. *Int J Hydrogen Energy* 2017;42:15064–72.
- [51] Eshghi A, Kheirmand M. Electroplating of Pt–Ni–Cu nanoparticles on glassy carbon electrode for glucose electro-oxidation process. *Surf Eng* 2019;35:128–34.

- [52] Er OF, Caglar A, Kivrak H. Enhanced electrochemical glucose oxidation in alkaline solution over indium decorated carbon supported palladium nanoparticles. *Mater Chem Phys* 2020;254:123318.
- [53] Brouzgou A, Lo Vecchio C, Baglio V, Aricò AS, Liang ZX, Demin A, Tsiakaras P. Glucose electrooxidation reaction in presence of dopamine and uric acid over ketjenblack carbon supported PdCo electrocatalyst. *J Electroanal Chem* 2019;855:113610.
- [54] Brouzgou A, Gorbova E, Wang Y, Jing S, Seretis A, Liang Z, Tsiakaras P. Nitrogen-doped 3D hierarchical ordered mesoporous carbon supported palladium electrocatalyst for the simultaneous detection of ascorbic acid, dopamine, and glucose. *Ionics* 2019;25:6061–70.
- [55] Balkourani G, Damartzis T, Brouzgou A, Tsiakaras P. Cost effective synthesis of graphene nanomaterials for non-enzymatic electrochemical sensors for glucose: a comprehensive review. *Sensors* 2022;22:355.
- [56] Brouzgou A, Tsiakaras P. Electrocatalysts for glucose electrooxidation reaction: a review. *Top Catal* 2015;58:1311–27.
- [57] Baumann TF, Worsley MA, Han TY-J, Satcher Jr JH. High surface area carbon aerogel monoliths with hierarchical porosity. *J Non-Cryst Solids* 2008;354:3513–5.
- [58] Pandolfo AG, Hollenkamp AF. Carbon properties and their role in supercapacitors. *J Power Sources* 2006;157:11–27.
- [59] Cui Q, Chao S, Bai Z, Yan H, Wang K, Yang L. Based on a new support for synthesis of highly efficient palladium/hydroxyapatite catalyst for ethanol electrooxidation. *Electrochim Acta* 2014;132:31–6.
- [60] Shi C, Lv C, Wu L, Hou X. Porous chitosan/hydroxyapatite composite membrane for dyes static and dynamic removal from aqueous solution. *J Hazard Mater* 2017;338:241–9.
- [61] Xu J, White T, Li P, He C, Han Y-F. Hydroxyapatite foam as a catalyst for formaldehyde combustion at room temperature. *J Am Chem Soc* 2010;132:13172–3.
- [62] Safavi A, Abbaspour A, Sorouri M, Mohammadi A. Highly efficient ethanol electrooxidation on a synergistically active catalyst based on a Pd-loaded composite of hydroxyapatite. *Chemelectrochem* 2016;3:558–64.
- [63] Zhao K, Qiao B, Wang J, Zhang Y, Zhang T. A highly active and sintering-resistant Au/FeOx–hydroxyapatite catalyst for CO oxidation. *Chem Commun* 2011;47:1779–81.
- [64] Tounsi H, Djemal S, Petitto C, Delahay G. Copper loaded hydroxyapatite catalyst for selective catalytic reduction of nitric oxide with ammonia. *Appl Catal B Environ* 2011;107:158–63.
- [65] Safavi A, Abbaspour A, Sorouri M. Hydroxyapatite wrapped multiwalled carbon nanotubes composite, a highly efficient template for palladium loading for electrooxidation of alcohols. *J Power Sources* 2015;287:458–64.
- [66] Zhao X, Xu D, Liu K, Dai P, Gao J. Remarkable enhancement of PdAg/rGO catalyst activity for formic acid dehydrogenation by facile boron-doping through NaBH4 reduction. *Appl Surf Sci* 2020;512:145746.
- [67] Ulas B, Caglar A, Yilmaz S, Ecer U, Yilmaz Y, Sahan T, Kivrak H. Towards more active and stable PdAgCr electrocatalysts for formic acid electrooxidation: the role of optimization via response surface methodology. *Int J Energy Res* 2019;43:8985–9000.
- [68] Alshemary AZ, Akram M, Goh Y-F, Abdul Kadir MR, Abdolah A, Hussain R. Structural characterization, optical properties and in vitro bioactivity of mesoporous erbium-doped hydroxyapatite. *J Alloys Compd* 2015;645:478–86.
- [69] Caglar A, Ulas B, Sahin O, Demir Kivrak H. Few-layer graphene coated on indium tin oxide electrodes prepared by chemical vapor deposition and their enhanced glucose electrooxidation activity. *Energy Storage* 2019;1:e73.
- [70] Wang J-C, Cheng F-C, Liang Y-T, Chen H-I, Tsai C-Y, Fang C-H, Nee T-E. Anomalous luminescence phenomena of indium-doped ZnO nanostructures grown on Si substrates by the hydrothermal method. *Nanoscale Res Lett* 2012;7:270.
- [71] Wang Q, Chen F, Tang Q, Guo L, Jin T, Pan B, Wang J, Li Z, Kou B, Bian W. AgPdCo hollow nanospheres electrocatalyst with high activity and stability toward the formate electrooxidation. *Nano Res* 2021;14:2268–76.
- [72] Carmody O, Frost R, Xi Y, Kokot S. Surface characterisation of selected sorbent materials for common hydrocarbon fuels. *Surf Sci* 2007;601:2066–76.
- [73] Ranganathan K, Morais A, Nongwe I, Longo C, Nogueira AF, Coville NJ. Study of photoelectrochemical water splitting using composite films based on TiO2 nanoparticles and nitrogen or boron doped hollow carbon spheres as photoanodes. *J Mol Catal Chem* 2016;422:165–74.
- [74] Bourlier Y, Bouttemy M, Patard O, Gamarra P, Piotrowicz S, Vigneron J, Aubry R, Delage S, Etcheberry A. Investigation of InAlN layers surface reactivity after thermal annealings: a complete XPS study for HEMT. *ECS J Solid State Sci Technol* 2018;7:P329.
- [75] Shi B, Su Y, Duan Y, Chen S, Zuo W. A nanocomposite prepared from copper(II) and nitrogen-doped graphene quantum dots with peroxidase mimicking properties for chemiluminescent determination of uric acid. *Microchim Acta* 2019;186:397.
- [76] Ruch P, Cericola D, Foelske-Schmitz A, Kötz R, Wokaun A. Aging of electrochemical double layer capacitors with acetonitrile-based electrolyte at elevated voltages. *Electrochim Acta* 2010;55:4412–20.
- [77] Zhang L, Ding L-X, Luo Y, Zeng Y, Wang S, Wang H. PdO/Pd-CeO2 hollow spheres with fresh Pd surface for enhancing formic acid oxidation. *Chem Eng J* 2018;347:193–201.
- [78] Casado-Rivera E, Gal Z, Angelo A, Lind C, DiSalvo FJ, Abruna HD. Electrocatalytic oxidation of formic acid at an ordered intermetallic PtBi surface. *ChemPhysChem* 2003;4:193–9.
- [79] Wang W, Dong Y, Xu L, Dong W, Niu X, Lei Z. Combining bimetallic-alloy with selenium functionalized carbon to enhance electrocatalytic activity towards glucose oxidation. *Electrochim Acta* 2017;244:16–25.
- [80] Hassan KM, Khalifa Z, Elhaddad GM, Abdel Azzem M. The role of electrolytically deposited palladium and platinum metal nanoparticles dispersed onto poly(1,8-diaminonaphthalene) for enhanced glucose electrooxidation in biofuel cells. *Electrochim Acta* 2020;355:136781.
- [81] Vasileva A, Haschke S, Mikhailovskii V, Gitlina A, Bachmann J, Manshina A. Direct laser-induced deposition of AgPt@C nanoparticles on 2D and 3D substrates for electrocatalytic glucose oxidation. *Nano-Struct, Nano Objects* 2020;24:100547.
- [82] Elkholy AE, Heikal FE-T, El-Said WA. Improving the electrocatalytic performance of Pd nanoparticles supported on indium/tin oxide substrates towards glucose oxidation. *Appl Catal Gen* 2019;580:28–33.
- [83] Ozok O, Kavak E, Er OF, Kivrak H, Kivrak A. Novel benzothiophene based catalyst with enhanced activity for glucose electrooxidation. *Int J Hydrogen Energy* 2020;45:28706–15.
- [84] Caglar A, Ulas B, Sahin O, Kivrak H. Synthesis of in situ N-, S-, and B-doped few-layer graphene by chemical vapor deposition technique and their superior glucose electrooxidation activity. *Int J Energy Res* 2019;43:8204–16.
- [85] Hamad AR, Calis H, Caglar A, Kivrak H, Kivrak A. Indole-based novel organic anode catalyst for glucose electrooxidation. *Int J Energy Res* 2022;46:1659–71.
- [86] Hu J, Lu H, Li M, Xiao G, Li M, Xiang X, Lu Z, Qiao Y. Cobalt valence modulating in CoOx incorporated carbon nanofiber for enhanced glucose electrooxidation. *Mater Rep: Energy* 2022;100091.
- [87] Obradović MD, Tripković AV, Gojković SL. The origin of high activity of Pt–Au surfaces in the formic acid oxidation. *Electrochim Acta* 2009;55:204–9.